Journal of Coastal Research	32	2	301–314	Coconut Creek, Florida	March 2016

Analysis of Sedimentation Problems at the Entrance to Mar del Plata Harbor

Raúl A. Cáceres[†*], Julio A. Zyserman[‡], and Gerardo M. E. Perillo[§]

[†]Departamento de Hidráulica
Facultad de Ingeniería
Universidad Nacional de La Plata
La Plata, Buenos Aires B1900,
Argentina

[‡]DHI Water & Environment, Inc.
Solana Beach, CA 92075, U.S.A.

[§]Departamento de Geología
Universidad Nacional del Sur
CONICET-Instituo Argentino de Oceanografía
Bahía Blanca, Buenos Aires B8000,
Argentina

www.cerf-jcr.org

www.JCRonline.org

ABSTRACT

Cáceres, R.A.; Zyserman, J.A., and Perillo, G.M.E. 2016. Analysis of sedimentation problems at the entrance to Mar del Plata Harbor. *Journal of Coastal Research,* 32(2), 301–314. Coconut Creek (Florida), ISSN 0749-0208.

Mar del Plata Harbor is an important center for the fishery industry in Argentina, and it has become an attractive site for international tourism because of the recent construction of a cruiser ship terminal. However, further development of this port halted several years ago because of the recurrent sedimentation problems in the access channel and basins. This site is characterized by advancement of the shoreline south of the harbor and a sandbank that develops across the access channel, while downdrift erosion and the associated shoreline retreat are due to partial blockage of the sediment transport caused by the harbor breakwaters. The mechanisms responsible for these sedimentation and erosion processes are examined using a coastal area morphological modeling system, MIKE 21/3 Coupled Model Flexible Mesh, developed by DHI. The morphological model was calibrated and validated against measured bathymetric changes. The model was then applied to a medium-term simulation with particular interest in the assessment of the effectiveness of re-establishing the design depth of the access channel through dredging. This morphological modeling allowed enhanced understanding of the main hydrodynamic and sedimentological processes occurring around the harbor entrance, as well as obtainment of information potentially useful for maintenance dredging. It was determined for the present hydrosedimentological conditions that the sandbank moves toward the access channel with high sedimentation rate. This means the navigation channel requires regular maintenance dredging or the construction of additional sediment retention interventions such as sediment traps, extension of the breakwater(s), *etc*. The efficiency of any intervention from the point of view of reducing sediment deposition at the harbor access should be verified before its implementation. In all cases, the northward transport would still be blocked, so artificial sediment bypass should be considered to protect the beaches north of the harbor.

ADDITIONAL INDEX WORDS: *Waves, sediment transport, numerical models, dredging, breakwaters*.

INTRODUCTION

It is known that assessment of the performance of coastal structures for design purposes requires detailed analyses and understanding of the interaction between the local hydrodynamics and the structures, as well as the sedimentological characteristics of the study area. However, sedimentation problems are often associated with human interference on the physical system, such as the construction of coastal structures or harbors. Consequently, although the design and construction of harbors is one of the oldest branches of civil engineering, maintaining sufficient navigation depth in front of the entrances is a frequent problem for many harbors; these projects can also lead to erosion problems at other nearby coastlines (van Rijn, 2005).

For example in Fortaleza, on the NE coast of Brazil, interconnected problems of sedimentation and erosion have been caused by the construction of a harbor in Mucuripe Bay (Maia *et al*., 1998). The harbor design did not take the longshore sediment transport into consideration, and port operations were consequently strongly affected by ensuing sedimentation (port siltation with excessive limitation of navigation depths) and downdrift beach erosion due to the partial blockage of the littoral drift caused by groynes and breakwaters. The area is characterized by a large sediment supply with a net longshore sediment transport, and to solve the port siltation, successive interventions were planned to deal with the sediment problems. From a harbor operation point of view, these modifications improved the situation, although periodical dredging was still required. However, from a coastal stability point of view, the erosive situation persisted. Expected economic benefits were apparently the main priority for planners, and little attention was paid to the erosion problem (the main interest was to prevent port siltation and not to mitigate coastal erosion). The interest in reversing or stopping coastal degradation only arose when a new coastal use (tourism), with more potential economic importance than the previous use, was identified.

Similar sedimentation problems affected the Thorsminde Harbor entrance, on the West Coast of Jutland, Denmark (Brøker *et al*., 2007). This port is located on a very exposed coastline, with a southward net littoral drift of about 0.4 million m^3/y, and the gross transport is several times larger. A new harbor layout was developed using the principles of natural

DOI: 10.2112/JCOASTRES-D-14-00056.1 received 18 March 2014; accepted in revision 28 August 2014; corrected proofs received 6 October 2014.

*Corresponding author: raul.caceres@ing.unlp.edu.ar

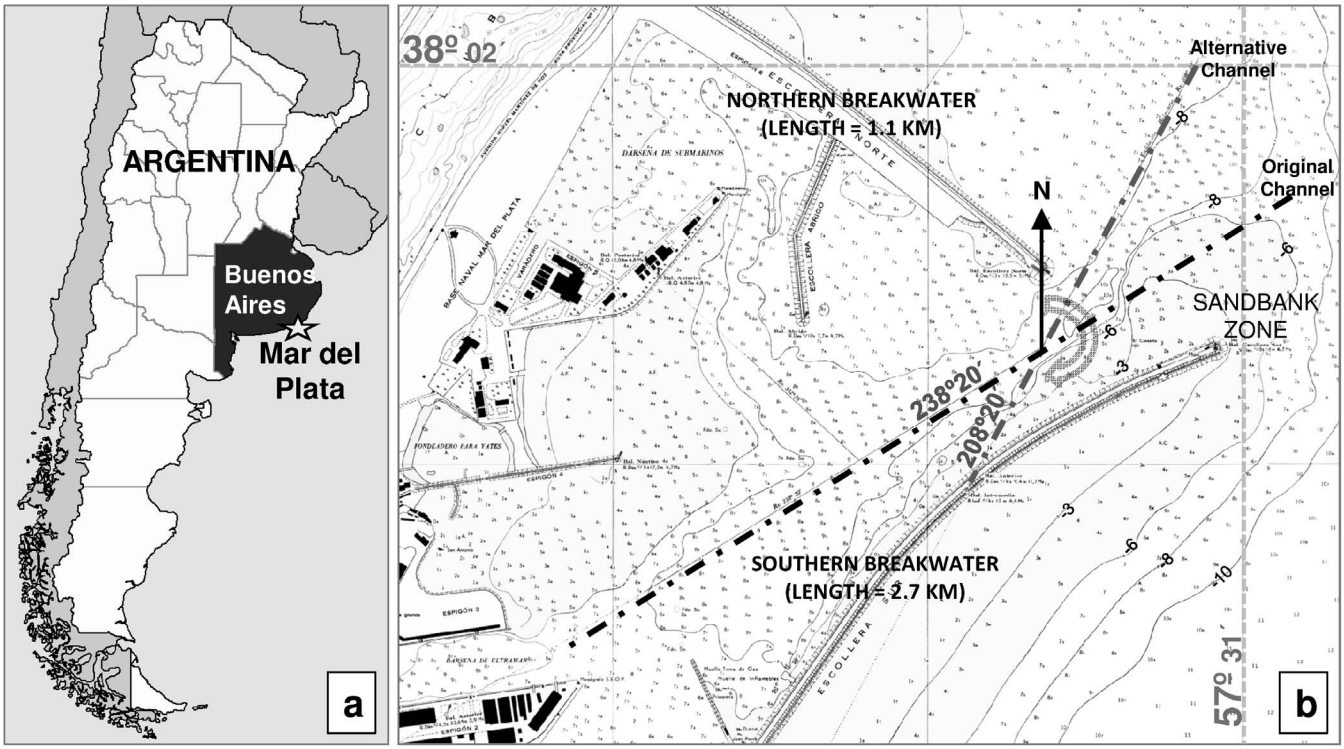

Figure 1. (a) General location of Mar del Plata Harbor. (b) Breakwaters, sandbank zone, original and alternative channel access in the Mar del Plata harbor. (Background image: Nautical Chart H251, Servicio de Hidrografía Naval (SHN), Argentina)

bypass, which is obtained when the sediment transport capacity in front of the harbor entrance is similar to the updrift littoral transport capacity (Mangor and Fuchs, 1999). The new breakwater was finished in the autumn of 2004 (Mangor *et al*., 2010). The first two following winters, a reduction in maintenance dredging to about 40% of the preconstruction volume was observed. However, in the following 3 years the maintenance dredging requirements increased again up to the levels before the construction of the new layout. The changes in harbor layout were not capable of maintaining the improved conditions for sediment bypass, because the bathymetry around the harbor gradually adjusted to the new conditions through an offshore movement of the depth contours updrift, which then resulted in reduced transport capacity in front of the entrance.

The aim of this paper is to investigate the hydrosedimentological processes occurring in the vicinity of an existing harbor and their effects on the morphology of the adjacent coastlines. For this purpose, Mar del Plata Harbor in Buenos Aires Province, Argentina, was selected (Figure 1a).

Mar del Plata Harbor was built with one main protective structure (Southern Breakwater) and a secondary structure (Northern Breakwater). Northward sediment transport is trapped at the harbor entrance, and a sandbank develops across the access channel. In view of this situation, the Port Authorities modified the original leading line from 238°20′ to 208°20′ (measured clockwise from North) to avoid in part the problem of reduced navigation depths (SHN, 2004) (Figure 1b).

Capital dredging of the sandbank and access channel occurred in 1998, with the dual goal of re-establishing the design depths at the harbor entrance and utilizing the dredged material as nourishment for the starved beaches north of the harbor. However, the harbor entrance became rapidly silted, and the beaches were eroded as well. A water depth of around 11 m and channel width of 100 m are required at the entrance to allow safe access for cargo ships calling at Mar del Plata Harbor. The present depth of the alternative channel access equals approximately 8.5 m (SHN, 2013).

The question as to which interventions would be required to re-establish the original depth of the access channel arises, together with the expected efficiency of any intervention. From the above discussion, it is apparent that the environmental and morphological conditions under which sedimentation problems occur at Mar del Plata Harbor's entrance have not yet been fully investigated, are not well understood, or both. The main objective of the present paper is therefore to gain enhanced understanding of the main hydrographic and sedimentological processes occurring at the harbor entrance and to assess the effectiveness of re-establishing the design depth through dredging. Both goals are achieved through the implementation of a numerical morphological model covering the area of interest for the study.

METHODS

The following section is structured in two parts. The first describes the study site and environmental conditions. The

second presents the coastal area morphological modeling system applied in the investigation and the bathymetric data used for the simulations.

Study Site

The coast of Mar del Plata is exposed to the South Atlantic Ocean wave climate; the net littoral drift is around 390,000 m^3/y (Caviglia, Pousa, and Lanfredi, 1992) and directed northward (Bertola, 2006; Isla, 2006). Shoreline retreat ranges from 0.5 m/y in some stretches to 5 m/y in others, which is attributed to physical factors (sea level fluctuations associated with storms from the south and southeast, combined with the presence of narrow beaches with limited availability of sand) and, indirectly, to human activity (Bertola, 2006).

Mar del Plata Harbor has had significant influence on its hinterland since its construction in the early 20th century with the development of fisheries and tourism. One of the main operative bases of the Argentinean Navy was established in the harbor, and many nautical and sports activities flourished. However, further development of this port has been limited for several years by the recurrence of sedimentation problems in the access channel and basins.

Before the Mar del Plata Harbor was constructed (1913–1922), there were no signs of beach accretion at the site. Following construction of the harbor, there have been significant changes in coastal morphology, with advancement of the shoreline south of the harbor as a result of accretion and downdrift erosion and associated shoreline retreat to the north from partial blockage of the littoral drift caused by the harbor breakwaters.

Nearly 14 years after construction, a bar started to hinder the harbor entrance. Dredging activities were first performed in 1950 (Caviglia, Pousa, and Lanfredi, 1992). In the 1970s, a dynamic equilibrium condition appeared to have been reached, because the hydrographic surveys showed that changes of the 9–11-m isobath lines along the main breakwater were already very small (SHN, 1975a,b). Consequently, it may be assumed that the South Breakwater had already reached its maximum capacity of interrupting the littoral drift, and a large fraction of the sediments in the littoral zone were transported toward the harbor entrance.

Moreover, the layout of the harbor breakwaters and orientation of the neighboring beaches meant that natural bypass of sediments toward the northern beaches could never happen. Therefore, sand supply to and retention on the beaches north of the harbor became a priority for local and provincial authorities, which lead to construction of a series of groynes. As more sand was retained by the urban beaches, erosion extended to other beaches further north, thus requiring construction of more groynes (Syvitski *et al.*, 2005).

Physical Setting

A subhumid template climate characterizes Mar del Plata city. Mean annual temperature is 13.9°C with precipitation of 864 mm/y. Coastal showers and rough seas, as well as strong squalls, episodically occur from extratropical storms originating in the South Atlantic Ocean, the so-called "*sudestadas*." The coast has a microtidal regime; open ocean average wave height is about 1.0 m. The environmental conditions at the study site (tides, currents, and wave climate) and bed sediment characteristics are presented in detail in the following sections; these conditions are then used for the numerical modeling analysis presented in the following section.

Tides

Astronomical tide at Mar del Plata is mixed, predominantly semidiurnal. The mean sea level is +0.91 m, mean high tide is +1.32 m, mean low tide is +0.52 m (all water levels are referred to Mar del Plata Harbor datum [HD]), and mean tidal range is 0.8 m. An analysis of the time series of hourly water levels recorded by the Servicio de Hidrografía Naval (SHN), Argentina, for the period 2008–2010 at Mar del Plata Harbor was carried out as part of the present study. More than 95% of the levels were less than +1.75 m HD, whereas 50% of them were less than +0.95 m HD. The highest level observed was +3.04 m HD in 2009, which reveals the presence of a meteorological tide of at least 1 m above the astronomical tide.

Tidal Currents

As part of a plan to remodel the Mar del Plata Harbor (Sunrise Technical Consultants, 1971), wave, currents, and water level measurements were performed for 13 months at the harbor entrance at a depth of 11.5 m in front of the Southern Breakwater. It was observed that tidal currents are predominantly northward during flood and southward during ebb. However, as a result of diurnal inequality, the current direction reversed for the smaller tidal amplitudes. The maximum values of tidal current speed recorded over this 13-month period were around 0.6 m/s near the surface and 0.2 m/s near the seabed.

The influence of waves on the measured currents was also investigated. It was observed that an increase in wave height resulted in an increase of the total current speed close to the bed, and that the current direction departed from the usual pattern for tidal currents. This was interpreted as a predominance of the wave-driven currents as the wave height increases. Currents were also measured within the surf zone and showed no influence from the tide. Waves from SSE and SE generated northward littoral currents, whereas waves from ESE, E, and ENE forced southward currents. The maximum recorded current speed was approximately 1 m/s.

Finally, the study carried out by Sunrise Technical Consultants (1971) investigated the currents driven by water level differences between the harbor basin and the sea. The maximum speeds recorded were around 0.2 m/s near the surface and almost zero at the bottom.

Therefore, tidal currents were assumed as being negligible from the point of view of local morphological changes in the vicinity of the harbor entrance and were discarded in the numerical model computations. In fact, the most important currents in the nearshore zone are longshore currents driven by breaking waves, whereas in offshore areas, all other types of currents, such as tidal currents and those generated by meteorological effects, are more important (Dean and Dalrymple, 2004).

Waves

Engineering projects in coastal areas require, among other factors, knowledge about local wave conditions. When wave measurements at the site are not available, alternative sources

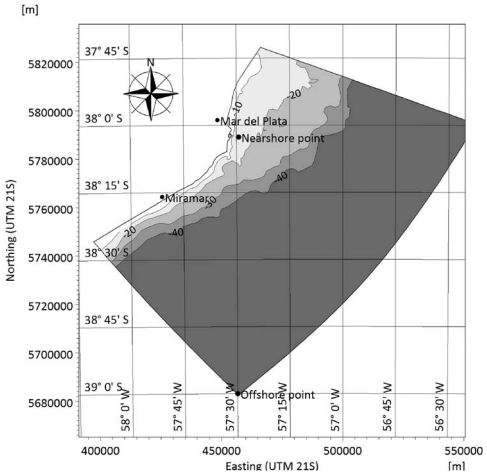

Figure 2. Bathymetry and location of the points for transformation of offshore waves (coordinates: 39.0° S, 57.5° W) into nearshore waves (coordinates: 38°2′38.07″; S, 57°29′24.20″ W).

of information must be used. Global Wave Models represent a suitable option; they are used by some European and U.S. agencies, especially for surf forecasting, harbor planning, and other maritime operations (Alves, Chao, and Tolman, 2005; Chini *et al*., 2010; Durrant and Greenslade, 2011; Etala *et al*., 2012; Papadopoulos, Katsafados, and Kallos, 2002).

In recent years, numerical modeling has made significant steps in forecasting waves at global and regional scales. Wave prediction/hindcasting models have been improved and shown their reliability through the successful development of third-generation wave models such as WAM, SWAN, and WAVEWATCH III (Booij, Ris, and Holthuijsen, 1999; Chawla *et al*., 2013; De Jong, 1997; Dragani *et al*., 2008; Padilla Hernández *et al*., 2007). Additionally, accurate and reliable meteorological data has been available for several decades from international organizations such as the European Centre for Medium-Range Weather Forecasts and the National Centers for Environmental Prediction (NCEP) (Saha *et al*., 2010).

Simulation/hindcast of ocean waves by means of wave models using meteorological data has thus become commonplace in recent years. Accurate and reliable historical wave information can be obtained for extended periods of time in many coastal areas where no measured wave data are available (Calverley *et al*., 2002; Camarena Calderon, 2012; Castellano, Tomazin, and Granada, 2009; Chini *et al*., 2010; Kassem and Özkan-Haller, 2012; Sclavo *et al*., 2000; Scott, Del Core, and Murty, 2000).

Hindcast time series data from NOAA's WAVEWATCH III Global Wave Model were used in the present study. The global model provides data at an offshore location (39.0° S, 57.5° W) about 100 km from Mar del Plata Harbor (Figure 2), including one value every 3 hours of total significant wave height (Hs), average wave period (Tm), peak wave period (Tp), and wave direction (MWD). A 3-year time series (2008–2010) was used in this study.

Hs-Tp distributions at the offshore location are presented in Table 1. Most significant wave heights occur in the range of 1.0–1.5 m (37.4% of occurrence) and are associated with significant wave periods between 6 and 10 seconds (65.1%). The principal directions of waves are S (11.7%), NE (10.7%), SSW (10.4%), SSE (9.4%), and ENE (9.4%).

Bed Sediments

The Mar del Plata coast is highly undulated with extended bay beaches between points of Devonian orthoquartzitic rocks (Syvitski *et al*., 2005). Some beaches are stable, whereas others have originated from human intervention (breakwaters, groynes, sand nourishments). Around Mar del Plata city, Pleistocene loess cliffs (up to 25 m high) are a significant source of sediment for littoral transport. Mar del Plata harbor was constructed in the Ensenada Mogotes between two headlands. The sediments of this beach are composed of medium to very fine sand (Isla *et al*., 1994).

Two sediment data sets (provided by Departamento de Costa Marítima de la Dirección Provincial de Saneamiento y Obras Hidráulicas, Buenos Aires Province, Argentina) were used in the present study. Sediment samples were collected from the crest of the sandbank at the harbor entrance. The characteristic particle sizes were: $d_{50}=0.21$ mm, $d_{84}=0.30$ mm, and $d_{16}=0.13$ mm, and the geometrical standard deviation or spreading was: $\sigma_g=(d_{84}/d_{16})^{0.5}=1.57$.

Numerical Model

The coastal area morphological modeling system MIKE 21 developed by DHI was used in the present study. The Coupled Model Flexible Mesh (FM) modeling system is described in detail in DHI (2011a–c) and, hence, is only briefly presented below.

Model Components

MIKE 21 FM consists of simulation modules for flow (hydrodynamic model, MIKE 21 HD), spectral waves (spectral wave model, MIKE 21 SW), and noncohesive sediment transport (sand transport model, MIKE 21 ST). All models are based on a numerical approach consisting of a cell-centered finite volume technique on an unstructured mesh consisting of triangular and/or quadrangular elements of different sizes. The same bathymetry model is used by all of the modules involved in the simulation.

The hydrodynamic model solves the two-dimensional Reynolds-averaged Navier–Stokes equations invoking the approximations of Boussinesq and hydrostatic pressure to compute the time and spatial variation of total water depth and depth-averaged velocity components. This involves simultaneously solving the continuity, momentum, temperature, salinity, and density equations (DHI, 2011a).

The spectral wave model simulates the growth, decay, and transformation of wind-generated waves and swell in offshore and coastal areas. This model also includes two different formulations for the wave action balance equation: directional decoupled parametric formulation and fully spectral (DHI, 2011b).

MIKE 21 ST FM makes use of the STPQ3D sediment transport model to compute rates of noncohesive sediment transport under combined waves and current. STPQ3D

Table 1. *WAVEWATCH III hindcast wave data at offshore location (39.0° S, 57.5° W), about 100 km from Mar del Plata harbor. Period analyzed: 2008–2010.*

	Tp (s)									
	0	2	4	6	8	10	12	14		
Hs (m)	2	4	6	8	10	12	14	16	Occurrence (%)	Exceedance (%)
0–0.5	0.0	0.0	0.0	0.1	0.0	0.0	0.0	0.0	0.1	99.90
0.5–1	0.0	0.3	2.6	5.4	4.4	0.7	0.3	0.1	13.7	86.18
1–1.5	0.0	0.0	8.2	10.8	14.1	3.8	0.4	0.0	37.4	48.75
1.5–2	0.0	0.0	5.1	5.5	10.4	4.9	0.5	0.0	26.4	22.36
2–2.5	0.0	0.0	0.5	3.4	4.7	3.1	0.3	0.0	12.1	10.30
2.5–3	0.0	0.0	0.0	1.7	2.3	1.9	0.1	0.0	6.0	4.27
3–3.5	0.0	0.0	0.0	0.3	0.9	0.9	0.2	0.0	2.3	2.00
3.5–4	0.0	0.0	0.0	0.0	0.6	0.4	0.1	0.0	1.1	0.87
4–4.5	0.0	0.0	0.0	0.0	0.2	0.2	0.0	0.0	0.5	0.39
4.5–5	0.0	0.0	0.0	0.0	0.1	0.2	0.1	0.0	0.4	0.03
5–5.5	0.0	0.0	0.0	0.0	0.0	0.0	0.0	0.0	0.0	0.03
5.5–6	0.0	0.0	0.0	0.0	0.0	0.0	0.0	0.0	0.0	0.01
6–6.5	0.0	0.0	0.0	0.0	0.0	0.0	0.0	0.0	0.0	0.00
6.5–7	0.0	0.0	0.0	0.0	0.0	0.0	0.0	0.0	0.0	0.00
Occurrence (%)	0.0	0.3	16.5	27.3	37.8	16.0	1.9	0.2	100	
Exceedance (%)	100	99.6	83.2	55.9	18.1	2.1	0.2	0.02		

provides a quasi–three-dimensional description of the force balance and hydrodynamics through the water column, as well as a detailed description of the instantaneous turbulent boundary layer under combined wave-current action. STPQ3D resolves the spatial (over the water column) and temporal (over the wave period) variations of bed shear stress, flow velocity, and sediment concentration using the integrated momentum approach of Fredsøe (1984) for the turbulent boundary layer. The total sediment load is split into bed load and suspended load, which are calculated separately. The transport of noncohesive material as bed load is calculated according to the model of Engelund and Fredsøe (1976) as a function of the instantaneous dimensionless bed shear stress or Shields parameter θ (Shields, 1936),

$$\theta = \frac{(u^*)^2}{(s-1)gd} \tag{1}$$

where s is the relative sediment density, g is the acceleration of gravity, d is the median grain size, and u^* is the shear velocity. The bed load transport is assumed to correspond to the instantaneous bed shear stress under unsteady conditions (*e.g.*, under combined action of current and waves).

The suspended load transport is described through the instantaneous suspended sediment concentration c, which is determined from the vertical turbulent diffusion equation, because horizontal diffusion terms are assumed small compared with the vertical diffusion terms:

$$\frac{\partial c}{\partial t} = \frac{\partial}{\partial t}\left(\varepsilon \frac{\partial c}{\partial z}\right) + w_s \frac{\partial c}{\partial z} \tag{2}$$

where t is time, z is the vertical coordinate measured upward from the bed, ε is the turbulent diffusion coefficient, and w_s is the settling velocity of the suspended sediment. The horizontal components of the average suspended sediment transport q_s over the wave period T are calculated as the product of sediment concentration and current velocity in the x and y directions, respectively (DHI, 2011c),

$$q_{sx} = \frac{1}{T}\int_0^T \left[\int_{2d}^{D} U_x(z,t) \times c(z,t) dz\right] dt \tag{3}$$

$$q_{sy} = \frac{1}{T}\int_0^T \left[\int_{2d}^{D} U_y(z,t) \times c(z,t) dz\right] dt \tag{4}$$

The effects of waves propagating at an arbitrary angle to the current, breaking/unbroken waves, uniform/graded bed sediment, plane/ripple-covered bed are taken into account when calculating the local rates of total load transport using STPQ3D. Spatial gradients in total load transport are used to compute the rates of bed level changes through the continuity equation for bed sediment, and the model bathymetry gets updated accordingly as the numerical model simulation proceeds.

In the coupled wave/current approach, the effects of wave setup and littoral currents are incorporated through the radiation stresses S_{xx}, S_{yy}, and S_{xy} from wave simulations with MIKE 21 SW. The resulting tensor field is passed on to the hydrodynamic model MIKE 21 HD, in which the radiation stress gradients ($\partial S_{xx}/\partial_x$, $\partial S_{yy}/\partial_y$, $\partial S_{xy}/\partial_y$) are used to drive littoral currents and wave setup/setdown. Wave parameters calculated by MIKE 21 SW and current velocity and water depth calculated by MIKE 21 HD are internally transferred to MIKE 21 ST for calculation of sediment transport rates. During the MIKE 21 ST simulations, the sediment transport rates associated both wave-induced and tidal currents are derived by interpolation from a precomputed lookup table generated using MIKE 21 Tools. The sediment transport table is precomputed for a range of wave/current/sediment parameters that cover the conditions of the modeling study. During the simulation, sediment transport rates are interpolated from the lookup table at every call to the sediment transport model.

Each of the modules in MIKE 21/3 Coupled Model FM use internal time steps, which are synchronized at an overall discrete time step defined by the user. The time steps for the

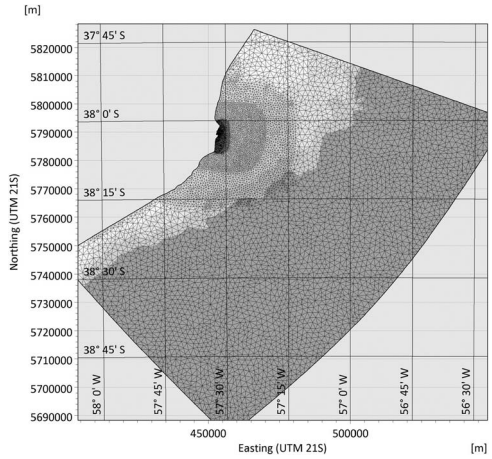

Figure 3. Computational mesh applied for the determination of wave climate close to Mar del Plata Harbor (the unstructured mesh consists of a total of 16,963 triangular elements and 8785 nodes).

hydrodynamic and the spectral wave calculations are dynamic and determined to satisfy stability criteria (*e.g.*, Courant–Friedrichs–Levy [CFL] number condition less than 1 for the hydrodynamic module) because of the explicit numerical scheme. The sediment transport rates are computed at the overall time step. In between calls to MIKE 21 ST, the bed levels in the model bathymetry are updated by extrapolating the rates of bed changes computed by the Sediment Transport Module at the previous time step.

Model Bathymetry

The following local surveys of the harbor entrance collected during 2009 were available for the creation of model bathymetries and for model calibration/validation purposes: January 12, February 24, April 14, May 27, July 15, August 5, September 24, October 28, November 23, and December 21. The surveys were performed using GPS differential corrections with submeter accuracy. The bathymetric survey was performed with a dual-frequency echo sounder (210 kHz/33 kHz). The vertical accuracy of the measurements was ± 0.10 m.

Because the local surveys only cover the access area of the harbor (the extension of these surveys is about 600×600 m and 400×400 m in the outer and inner area of the harbor entrance, respectively), additional bathymetric information covering a larger area was required to create the model bathymetry. Therefore, the following nautical charts from the Servicio de Hidrografía Naval were digitized to generate a digital elevation model:

- H210 ("De Faro Punta Mogotes Claromecó," scale 1:250,000)
- H250 ("Rada Mar del Plata," scale 1:50,000)
- H251 ("Puerto de Mar del Plata," scale 1:5000)

All nautical charts were digitized and georeferenced with DHI's MIKE Zero tools, and the processed chart data were compiled with the detailed survey of the port access. The detailed survey data were prioritized in the port access area.

RESULTS

The problem of sedimentation in the access channel to Mar del Plata Harbor was assessed through medium-term coastal area modeling with the morphological model MIKE 21 FM. To reduce the computational effort, the spectral wave MIKE 21 SW FM model was used for the transformation of WAVEWATCH III offshore waves into nearshore waves before executing the morphological model. In this way, it was possible to exercise the morphological model on a smaller area of higher mesh resolution.

The following section is structured in two parts. The first part presents the determination of the nearshore wave climate through simulations with MIKE 21 SW. The second part presents the calibration/validation and application of the coastal area morphological modeling system MIKE 21 Coupled Model (FM).

Determination of Nearshore Wave Climate

The time series of wave parameters hindcasted by NOAA's WAVEWATCH III model at the offshore location (39.0° S, 57.5° W) was transformed to a nearshore position close to Mar del Plata Harbor: 38°2′38.07″ S, 57°29′24.20″ W (Figure 2). The computational domain covers 110 km in the alongshore direction and 90 km in the offshore direction (Figure 3). The hindcasted time series of wave data were specified at the offshore boundary of the model domain. Symmetrical open-sea boundary conditions were invoked at the lateral model boundaries.

To optimize the mesh resolution, the computational domain was partitioned into four subdomains, with decreasing element size/increasing resolution toward the area of interest. The unstructured mesh consists of a total of 16,963 triangular elements with a spatial resolution of about 2000 m in offshore areas and 50–100 m in the nearshore region (see Figure 3 for details).

Because of the relatively large extent of the computational domain in the offshore dimension, wind wave growth was accounted for in the spectral wave model. The wind data used as input for the MIKE 21 SW FM model were obtained from hindcast archives of the NCEP's wave prediction system, consisting of analysis of data from the global atmospheric forecasting system at NCEP/NOAA (Moorthi, Pan, and Caplan, 2001). The data consist of wind speed and direction every three hours at the same offshore location as the WAVEWATCH III hindcast position (coordinates: 39.0° S, 57.5° W) and an elevation of 10 m.

Wave growth and wave propagation were computed using the fully spectral formulation in MIKE 21 SW with nonlinear wave-wave interactions and whitecapping. A logarithmic frequency discretization with 25 frequencies was adopted. The lowest discrete frequency is 0.05 Hz (corresponding to a maximum peak wave period of 20 s) and the ratio between successive frequencies was chosen as 1.1, resulting in a minimum wave period of 2.03 seconds. The number of discrete directions was chosen as 16 at 22.5° intervals. The overall time step in the simulation was chosen as 1800 seconds. Wave breaking was computed according to the Battjes and Janssen (1978) model with the following values: $\gamma_1 = 1.0$ (controls steepness breaking), $\gamma_2 = 0.8$ (controls depth-limited breaking),

Table 2. *Wave incidence in the vicinity of Mar del Plata Harbor. Period analyzed: 2008–2010.*

	Tp (s)									
	0	2	4	6	8	10	12	14		
Hs (m)	2	4	6	8	10	12	14	16	Occurrence (%)	Exceedance (%)
0–0.5	0.00	0.00	0.38	0.21	0.14	0.14	0.00	0.00	0.86	99.14
0.5–1	0.10	2.60	10.21	4.21	7.40	5.99	1.37	0.03	31.92	67.23
1–1.5	0.00	1.37	15.72	4.59	9.93	8.49	1.68	0.03	41.82	25.41
1.5–2	0.00	0.07	2.95	2.40	3.87	4.83	2.33	0.00	16.44	8.97
2–2.5	0.00	0.00	0.10	0.92	1.44	2.02	1.03	0.00	5.51	3.46
2.5–3	0.00	0.00	0.03	0.07	0.72	0.48	0.65	0.00	1.95	1.51
3–3.5	0.00	0.00	0.00	0.03	0.38	0.31	0.27	0.00	0.99	0.51
3.5–4	0.00	0.00	0.00	0.00	0.07	0.07	0.21	0.00	0.34	0.17
4–4.5	0.00	0.00	0.00	0.00	0.00	0.03	0.07	0.00	0.10	0.07
4.5–5	0.00	0.00	0.00	0.00	0.00	0.00	0.07	0.00	0.07	0.00
5–5.5	0.00	0.00	0.00	0.00	0.00	0.00	0.00	0.00	0.00	0.00
5.5–6	0.00	0.00	0.00	0.00	0.00	0.00	0.00	0.00	0.00	0.00
6–6.5	0.00	0.00	0.00	0.00	0.00	0.00	0.00	0.00	0.00	0.00
6.5–7	0.00	0.00	0.00	0.00	0.00	0.00	0.00	0.00	0.00	0.00
Occurrence (%)	0.10	4.04	29.38	12.43	23.94	22.36	7.67	0.07	100.00	
Exceedance (%)	99.90	95.86	66.47	54.04	30.10	7.74	0.07	0.00		

and $\gamma = 0.5$ (controls the rate of wave energy dissipation by breaking). Bed friction was included; a Nikuradse roughness $k_N = 0.04$ was applied. The effect of tidal level variations was also included in the wave simulation by use of hourly values of measured water levels provided by Argentina's Servicio de Hidrografía Naval. The time series of water levels were applied as varying in time and constant over the model domain.

The resulting nearshore wave climate is presented in Table 2. The most significant wave heights range between 1.0 and 1.5 m (42% of the total) and are associated with significant wave periods between 4 and 12 seconds (88% of the total). Waves from the S and SSE were most common (35% of the total), which is in agreement with wave conditions typically observed at Mar del Plata.

Morphological Model Setup

The first step in the morphological model set-up is the definition of the computational domain and the calculation mesh. The computational domain must be large enough to eliminate boundary effects within the area of interest for the wave and hydrodynamic models. Furthermore, boundary effects should be avoided to the greatest extent possible in the morphological model. On the other hand, size and spacing of the mesh elements determine the resolution of the mode domain. Models with larger element sizes tend to be more diffusive and, hence, introduce more uncertainty into their predictions (Jones, Petersen, and Kofoed-Hansen, 2007).

Therefore, the selected morphological model domain has a total length of approximately 6500 m along the coast and 4000 m perpendicular to the coast. To optimize the mesh resolution, the computational mesh was partitioned into eight subdomains, and the mesh size decreased (resolution increased) as it approached the area of interest. The resulting mesh consisted of 33,411 elements and 17,009 nodes in total. The maximum element length is 250 m and the minimum is 11 m. The model bathymetry was generated by interpolation of bed elevations from local surveys and digitized sea charts to the nodes of the unstructured mesh, as already mentioned in the "Model Bathymetry" section.

Offshore boundary conditions for the wave module correspond to the results provided by the offshore wave propagation model presented in the previous section, and the main wave model parameters adopted for the offshore wave model were maintained in the local wave model. However, a parametrically decoupled version of the model (DS model) was applied, rather than the full spectral wave formulation to keep computational run times within reasonable limits, the large number of model runs to be completed taken into account. The DS model removes time as a dependent variable and solves the wave action–balance equation as a steady state solution (Holthuijsen *et al.*, 1989). This model is further simplified by parameterization of the frequency space but retains the directional properties of the wave spectrum. Both parameterizations allow reducing the number of degrees of freedom from 125 to 25, and provide a fivefold decrease in the run time of the DS model, compared with a fully spectral wave model. An application and validation of the model can be seen in Jones, Petersen, and Kofoed-Hansen (2007).

As mentioned in a previous section, sediment transport rates are derived by linear interpolation in a sediment transport table of MIKE 21 Tools. In this precomputed table, Stokes fifth order wave theory was applied to describe the wave-induced near-bed velocities above the wave boundary layer. Small sediment transport rates (compared with the wave-driven sediment transport within the surf zone) are calculated by the sediment transport model as a result of wave asymmetry.

Water level time series (hourly values) were imposed as boundary conditions to MIKE 21 HD FM. Lateral boundary conditions were corrected for wave-generated setup and littoral currents using the radiation stresses calculated by the MIKE 21 SW FM model. Salinity variation at the boundaries was not included because constant water density was assumed in all model runs. A maximum computational time step of 1800 seconds was chosen for the simulations. As discussed in a previous section, the actual time step used by the wave and hydrodynamic modules is defined by the corresponding model based on internal conditions about stability of the numerical solution (DHI, 2011a).

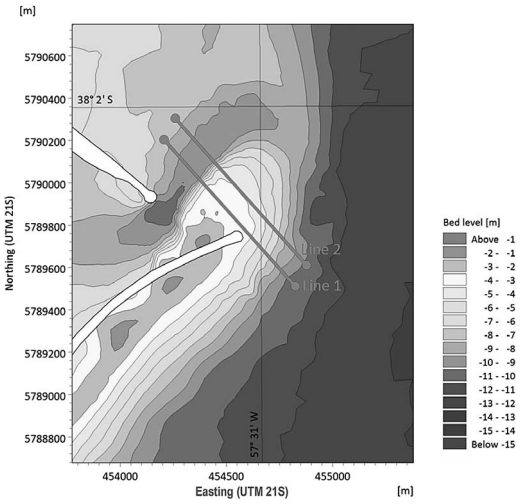

Figure 4. Bathymetry in the modeled area and control lines for simulations with MIKE 21 Coupled Model FM (UTM coordinate system).

Sediment properties were assumed constant throughout the model area. Based on the characteristics of the sediment samples collected on the sandbank, well-graded sand with median grain size, $d_{50} = 0.21$ mm and $\sigma_g = 1.57$, was adopted. The remaining model parameters were selected based on results from the calibration of the morphological model against bed level changes extracted from the local bathymetric surveys of the harbor entrance performed in 2009.

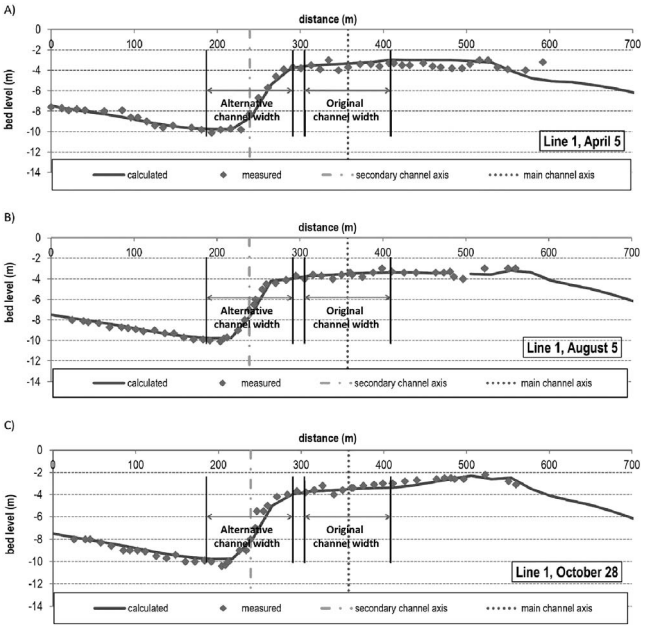

Figure 5. Comparison of measured and simulated bed levels in front of the harbor entrance along line 1—(A) results of the April 14, (B) August 5, and (C) October 28, 2009 surveys. Each chart shows the channel widths and relative position of the channel axis. The analysis consisted of a morphological simulation based on time series of wave parameters and water levels for a 1-y period (2009).

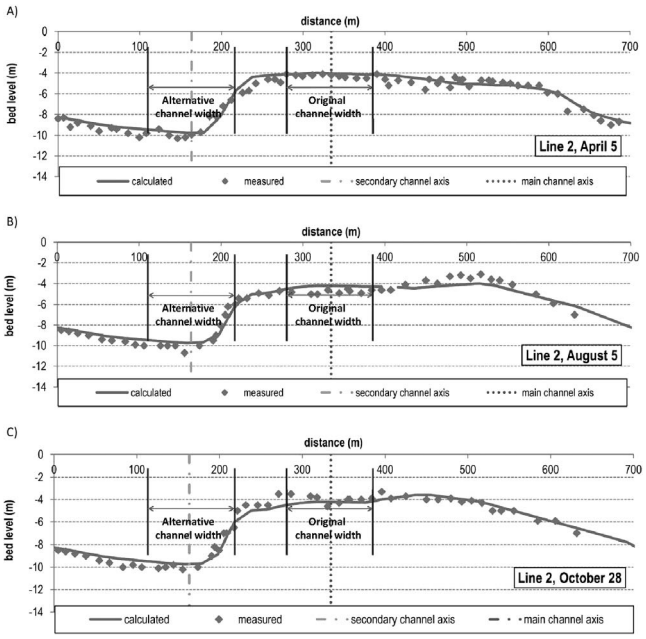

Figure 6. Comparison of measured and simulated bed levels in front of harbor entrance along line 2—(A) results of the April 14, (B) August 5, and (C) October 28, 2009 surveys. Each chart shows the channel widths and relative position of the channel axis. The analysis consisted of a morphological simulation based on time series of wave parameters and water levels for a 1-y period (2009).

Calibration/Validation of the Morphological Model

The morphological model was calibrated and validated against measured bathymetries of the harbor entrance. The analysis consisted of a morphological simulation based on time series of wave parameters and water levels for a 1-year period (2009) for which bathymetry surveys of the harbor entrance are available. The evolution of the sandbank over this period was analyzed in detail along two lines (Figure 4).

The best agreement between field measurements and model results was obtained for the following selection of model parameters: maximum morphological time step of 1800 seconds, eddy viscosity according to the Smagorinsky formulation with a spatially constant coefficient 0.8, and bed resistance in the hydrodynamic model defined as a constant Manning number $M = 45$ m$^{1/3}$/s for the entire computational domain. The simulation using these model parameters showed acceptable results (Figures 5 and 6), with 0.97 correlation between measured and calculated bed levels along lines 1 and 2.

Additionally, a comparison between the measured and observed bed level changes was performed (Figure 7). The correlation was also good, with value of 0.74.

Analysis of Hydrosedimentological Processes

The calibrated morphological model was applied to compute waves, currents, and sediment transport fields for stationary

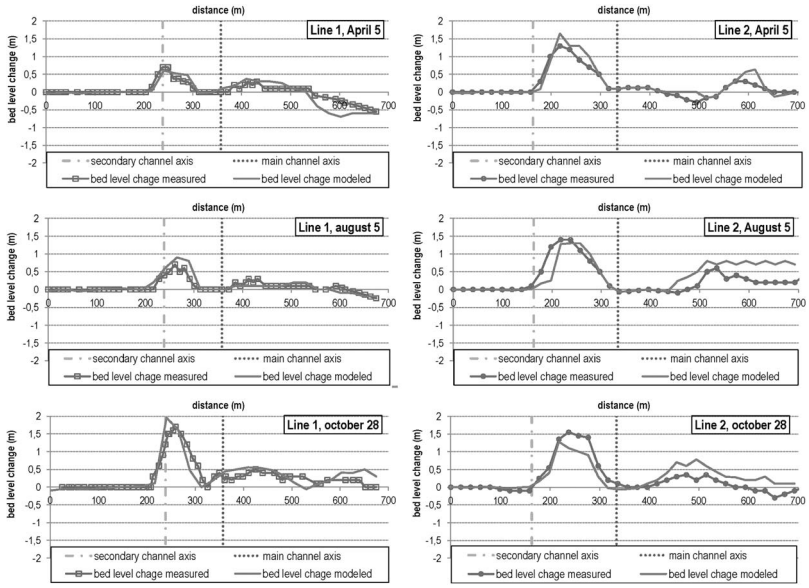

Figure 7. Comparison of measured and simulated bed levels changes in front of harbor entrance along line 1 and line 2—(A) results of the April 14, (B) August 5, and (C) October 28, 2009 surveys. Each chart shows the relative position of the channel axis.

wave and sea level conditions. The hydrodynamic and sedimentological processes that occur under these selected hydrodynamic conditions are discussed in detail in this section. The test cases discussed here were chosen to best illustrate the circulation patterns originated by incident waves from different directions. Contours of calculated significant wave height have been plotted together with vectors indicating the direction of wave propagation, as well as current patterns and bed level change (Figures 8 and 9).

For waves propagating from the SSE, SE, and E, the figures clearly show how the breakwater blocks the incident waves, creating a shadow area behind it (Figures 8A1 and A2 and 9A3). For incident waves from the NE, the wave energy is higher at the harbor entrance compared with waves propagating from the SSE, SE, and E (Figure 9A4).

For incident waves from the SSE direction, flow across the access channel is induced by wave breaking on the sandbank. Also, the results indicate the presence of a circulation pattern at the lee of the South Breakwater from flow separation driven by gradients in wave setup (Figure 8B1).

Similarly, for incident waves from the SE, the breaking process on the sandbank causes strong currents across the harbor entrance (Figure 8B2). These currents result in morphological changes (deposition) close to the access channel (Figures 8C2). As it was analyzed by Mangor and Fuchs (1999), these hydrodynamic patterns are the primary mechanism responsible for siltation in the port access zone. At the same time, the cross-currents create difficulties for navigation of vessels.

Under SSE and SE incident waves, currents parallel to the South Breakwater are generated (Figures 8B1 and B2). These currents are responsible for the transport of sand toward the tip of the breakwater and the harbor entrance (Figures 8C1 and C2).

For waves approaching from the E, flow divergence between both breakwaters also occurs, but in this case the circulation current occurs further inside the harbor than for waves from the S and SE (Figure 9B3). While waves from the S and SE tend to generate sediment deposition in the area of the access channel, the area where the sand deposits moves further inside the harbor under waves from the E (Figure 9C3).

When waves approach the harbor from the NE direction, the strongest currents occur on the inner side of the South Breakwater (Figure 9B4). This process will also be responsible for the transport of sediment into the harbor (Figure 9C4).

DISCUSSION

As was mentioned in the "Introduction," maritime harbors frequently face sedimentation problems in access channels and basins and, in most cases, also cause unwanted erosion in neighboring beaches. These phenomena are mainly related to the layout of the protective structures and their interaction with the local wave climate, the currents and the sediment transport. It is therefore important to understand the hydrodynamic processes and the effect of human interventions on the environment to avoid or minimize the effects on harbor performance (from wave agitation, sedimentation, or both in access channels and basins) and on coastal morphology (*i.e.* erosion of neighboring coastal areas).

Siltation of the Mar del Plata Harbor access is the result of accumulation of sediments originating from beaches to the South. This process extends along the entire length of the Southern Breakwater and manifests itself as a sandbank at its tip, which limits local water depths to 3 or 4 m. In recent years, this has had a negative effect on the port's economy because of

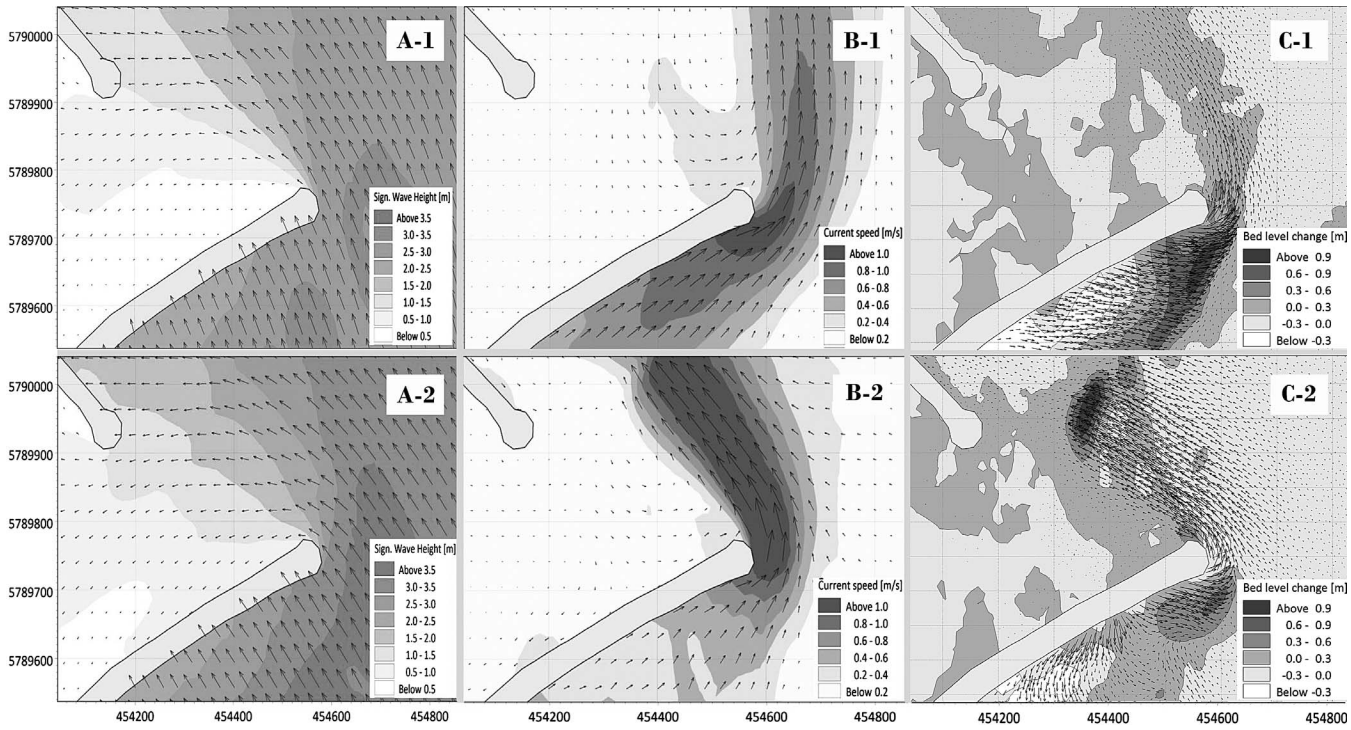

Figure 8. (A) Contours of wave height and direction (in the form of vector plots). (B) Wave-driven current fields in the form of vector plots and contours of depth-averaged current speed. (C) Contours of bed level change and sediment transport in the form of vector plots resulting for each incident wave. Subscript 1, incident wave from SSE; 2, incident wave from SE (UTM 21S coordinate system).

deep-draft vessel limitations of access to the port to load fishery products and general cargo containers for export purposes. Tourist cruise boats also experience problems in calling at the port, which has limited the number of these vessels, with ensuing losses for the tourism industry. Furthermore, because the harbor structures block a significant fraction of the northward sediment transport, the beaches to the north have experienced significant erosion problems (up to 5 m/y) from the reduced supply of sand (Isla, 2006). Erosion processes have affected not only tourism, but also the structural stability of houses and even of a road located in the vicinity of the coastline (Syvitski *et al*., 2005).

It can be reasonably argued that processes triggered by construction of the Southern Breakwater have resulted in a new morphological configuration and, therefore, in new hydro-morphological conditions, compared with those existing before its construction. This is because the shoreline south of the harbor advances by accumulation of sediment, pushing the active littoral zone offshore. The active zone is where measurable morphological changes larger than 10 cm occur (Nicholls *et al*., 1998). Results from our morphological modeling simulations show that the active littoral zone in the vicinity of the Southern Breakwater extends up to depths between 9 and 10 m. Therefore, the entire Southern Breakwater and the entrance to the harbor are located within a morphologically active area where sediments are in permanent movement, which will result in local erosion or deposition depending on the hydrodynamic conditions.

The question of interventions required to re-establish the original depth of the access channel arises, together with the expected efficiency of any intervention. The question may, to a certain extent, be answered by observations carried out at the harbor after dredging of the sandbank and access channel in 1998 with the goal of re-establishing the design depths and use of the dredged material as nourishment for the starved beaches north of the harbor. A few years later, the sandbank had recovered its initial volume and encroached on the access channel, where depths dropped to 4.8 m HD (SHN, 2004). As a consequence of this sedimentation, the sailing line followed by ships calling at the harbor had to be modified from its designed alignment of 238° to a secondary channel with an alignment of 208°, as shown in Figure 1b. This means that under prevailing hydrosedimentological conditions, the access channel will not be able to maintain the design depths without maintenance dredging and/or additional interventions such as sediment traps, sediment retention jetties, *etc*.

To assess the effectiveness of hypothetical dredging in the channel access, morphological simulation based on time series of wave parameters and water levels for a 3-year period (2008–2010) was performed. A hypothetical access channel with a bottom width of 110 m was dredged to a depth of 11 m (HD).

The lines shown in Figure 4 were used to assess the development of the sandbank and the access channel. After 3 years of simulation, the sandbank had migrated toward the access channel (Figures 10 and 11), with siltation rates at the location of the original channel's axis of 0.8 m/y and 0.6 m/y for

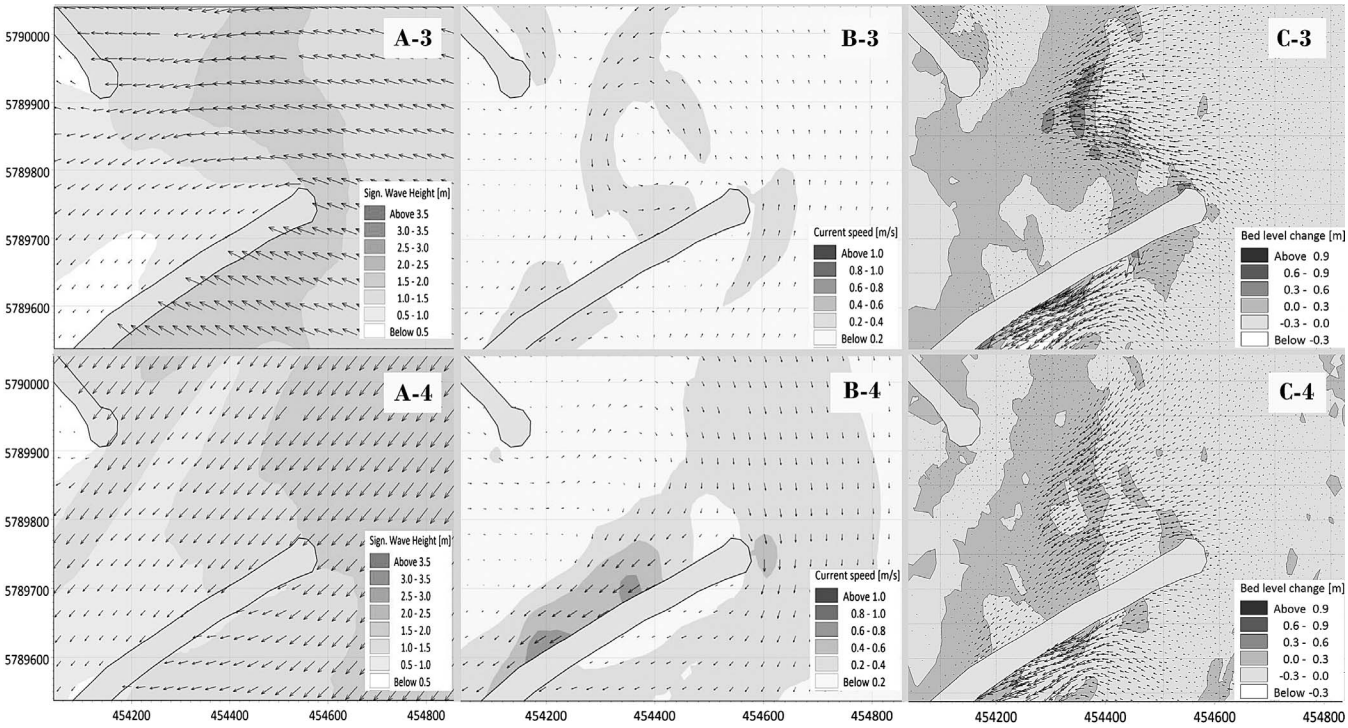

Figure 9. (A) Contours of wave height and direction (in the form of vector plots). (B) Wave-driven current fields in the form of vector plots and contours of depth-averaged current speed. (C) Contours of bed level change and sediment transport in the form of vector plots resulting for each incident wave. Subscript 3, incident wave from E; 4, incident wave from NE (UTM 21S coordinate system).

profiles 1 and 2, respectively. The rate of deposition is much higher on the left/upstream slope of the channel, up to 5 m/y.

The simulation results show that the water depth on top of the sandbank approaches 2 to 3 m along profile 1, and 4 to 5 m along profile 2. The depths within the access channel do not reach equilibrium after 3 years of simulation. However, the trend in the model results shows that the sediment deposition process tends to backfill the navigation channel up to a depth of 4 m (as was observed after the dredging in 1998). Sedimentation of the secondary/alternative channel is also observed, although at a slower rate than in the main channel.

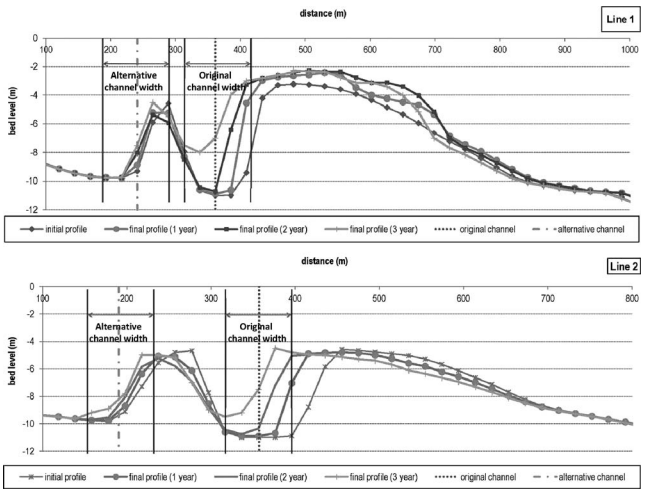

Figure 10. Profiles 1 and 2 across the sandbar and access channels calculated with the mathematical model for the period 2008–2010. Each chart shows the channel widths and relative position of the channel axis.

It should also be mentioned that the morphological model results in the outer zone of the South Breakwater are consistent with the historical morphological evolution of the area, where there is a relatively stable beach but alternative erosion and deposition areas may occur because of the wave climate.

The total sediment transport at the South Breakwater head was calculated through integration of model results across line 1. An average northward rate of 270,000 m^3/y was obtained over the 3 years covered by the simulation, together with an average southward transport rate of 25,000 m^3/y. Similarly, the total sediment transport along the main breakwater (across a section 400 m south of the breakwater head) was calculated. Average sediment transport rates of 345,000 m^3/y and 65,000 m^3/y were obtained for northward and southward components, respectively. This result is consistent with the investigation of Caviglia, Pousa, and Lanfredi (1992).

The volume of sediment deposited in the access channel was calculated as 255,000 m^3/y on average over the 3 years spanned by the simulation. This means that a large fraction of the northward sediment transport gets trapped in the access channel and cannot reach the beaches to the north of the

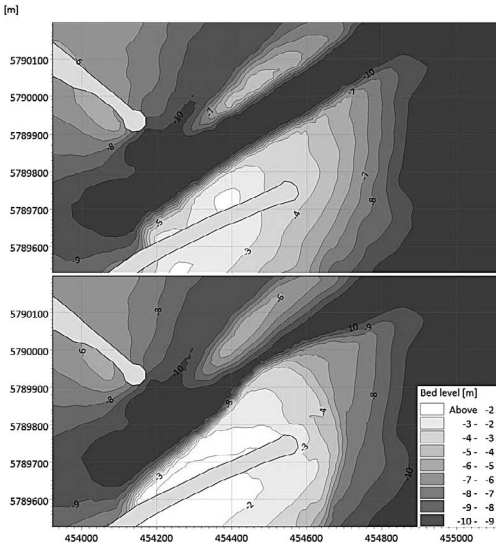

Figure 11. Evolution of bed level at Mar del Plata Harbor entrance after 3 y of morphological simulation (period 2008–2010). A hypothetical access channel with a bottom width of 110 m and a depth of 11 m (HD) was applied.

harbor, with the consequent effect on their morphology. The results also highlight the fact that regular maintenance dredging is required to maintain an access channel deeper than the natural depth. The efficiency of additional structures aimed at reducing sediment deposition at the harbor access, such as a sediment trap or jetties on the southern breakwater and perpendicular to it, should be verified before their implementation. In any case, the northward transport would still be blocked, so artificial sediment bypass should be considered to protect the beaches north of the harbor.

CONCLUSIONS

In this paper, results are presented from an analysis of coastal dynamics in the vicinity of a harbor entrance using a coastal area morphological model. The model was calibrated and validated against available bathymetric surveys of the harbor entrance. The numerical model, which simulates waves, currents, sediment transport, and corresponding bed level changes, has proven to be a useful tool in supporting the understanding of the processes around the harbor entrance.

From the results presented here, it is evident that the interaction between local hydrodynamics and sediment transport on the one side and the layout of protective works on the other side have caused persistent sedimentation at the entrance to Mar del Plata port. The entire littoral zone has been shifted offshore by the harbor breakwaters, which promotes the formation of a sandbank in the vicinity of the tip of the southern breakwater and sedimentation in the access channel. In this new situation, the question was posed as to whether the natural depth or equilibrium depth is greater or smaller than the required navigation depth.

The equilibrium depth at the harbor entrance has been evaluated using medium-term morphological modeling. It was determined that the sandbank moves toward the access channel and results in an elevated sedimentation rate. This means that for the present hydrosedimentological conditions, maintaining a navigation channel with depths greater than the equilibrium depth would require regular maintenance dredging or construction of additional sediment retention interventions such as sediment traps, extension of breakwater, *etc*.

The mathematical modeling exercise presented here also allowed the estimation of sediment transport rates along the Southern Breakwater. The calculated sediment transport rates across a section 400 m south of the breakwater head amounts to ~345,000 and ~65,000 m^3/y northward and southward, respectively. The gross sediment transport on the sandbank zone at the harbor entrance amounts to ~295,000 m^3/y, with ~255,000 m^3/y trapped by the access channel to the harbor. This results in well-known sedimentation problems for the harbor, as well as a sediment deficit for the beaches north of it. Any intervention aimed at combating or avoiding sedimentation of the access channel that does not resolve the problem of blocked littoral drift should therefore be disregarded.

ACKNOWLEDGMENTS

We thank reviewers of JCR for the time they spent revisiting our work and for their valuable suggestions. Thanks to Roberto Castellano of Instituto Nacional del Agua (INA), Argentina, for his detailed review of this work. The first author also thanks Belen Bergna for her assistance in reviewing the manuscript. Partial support was provided by a grant by Agencia Nacional de Promoción Científica y Tecnológica (ANPCYT) to Gerardo M.E. Perillo, and partial support was provided by a cofinanced grant by ANPCYT and INA to Raúl A. Cáceres. Finally, the support provided by DHI Water & Environment Inc. through the free Student License to Raúl A. Cáceres of the MIKE 21/3 Coupled Model is gratefully acknowledged.

LITERATURE CITED

Alves, J.H.G.M.; Chao, Y.Y., and Tolman, H.L., 2005. *The Operational North Atlantic Hurricane Wind-Wave Forecasting System at NOAA/NCEP*. Washington, DC: National Oceanic and Atmospheric Administration. *Technical Note No. 244*, 59p.

Battjes, J.A. and Janssen, J.P.F.M., 1978. Energy loss and set-up due to breaking of random waves. *Proceedings of the 16th International Conference on Coastal Engineering* (Hamburg, Germany, COPRI and ASCE), pp. 569–587.

Bertola, G., 2006. Morfodinámica de playas del Sudeste de la provincia de Buenos Aires (1983 a 2004). *Revista de la Asociación Argentina de Sedimentología* [*Latin American Journal of Sedimentology and Basin Analysis*], 13(1), 31–57 [in Spanish].

Booij, N.; Ris, R.C., and Holthuijsen, L.H., 1999. A third generation wave model for coastal regions, Part I, Model description and validation. *Journal of Geophysical Research,* 104(4), 7649–7666.

Brøker, I.; Zyserman, J.; Madsen, E.Ø.; Mangor, K., and Jensen, J., 2007. Morphological modelling: A tool for optimization of coastal structures. *Journal of Coastal Research,* 23(5), 1148–1158.

Calverley, M.J.; Szabo, D.; Cardone, V.J.; Orelup, E.A., and Parsons, M.J., 2002. Wave climate study of the Caribbean Sea. *7th International Workshop on Wave Hindcasting and Forecasting* (Banff, Alberta, Canada, Environment Canada, Canadian Federal Program of Energy R&D, WMO/IOC JCOMM), pp. 75–86.

Camarena Calderon, R.A., 2012. Feasibility of a Marina Port along the Buenos Aires Coast, Argentina. Delft, The Netherlands: Delft University of Technology, Master's thesis, 130p.

Castellano, R.D.; Tomazin, N.J., and Granada, J., 2009. Caracterización del clima de olas en el litoral marítimo de la Provincia del Chubut. *Congreso Nacional del Agua* (Trelew, Argentina, Comité Permanente de los Congresos del Agua and Provincia del Chubut), pp. 35–52.

Caviglia, F.J.; Pousa, J.L., and Lanfredi, N.W., 1992. Transporte de sedimentos: Una alternativa de cálculo. *II Congreso de Ciencias de la Tierra, Memorias* (Santiago, Chile, Instituto Geográfico Militar de Chile), pp. 413–422.

Chawla, A.; Tolman, H.L.; Gerald, V.; Spindler, D.; Spindler, T.; Alves, J.; Cao, D.; Hanson, J.L., and Devaliere, E.M., 2013. A multigrid wave forecasting model: A new paradigm in operational wave forecasting. *Weather and Forecasting*, 28(4), 1057–1078.

Chini, N.; Stansby, P.; Leake, J.; Wolf, J.; Roberts-Jones, J., and Lowe, J., 2010. The impact of sea level rise and climate change on inshore wave climate: A case study for East Anglia (UK). *Coastal Engineering,* 57(11–12), 973–984.

Danish Hydraulic Institute, 2011a. *MIKE 21 & MIKE 3 Flow Model FM. Hydrodynamic and Transport Module Scientific Documentation*. Horshølme, Denmark: DHI Water & Environment, Inc. *Scientific Documentation,* 52p.

Danish Hydraulic Institute, 2011b. *MIKE 21 Spectral Wave Module*. Horshølme, Denmark: DHI Water & Environment, Inc. *Scientific Documentation,* 66p.

Danish Hydraulic Institute, 2011c. *Noncohesive Sediment Transport in Currents and Waves*. Horshølme, Denmark: DHI Water & Environment, Inc. *Scientific Documentation,* 66p.

De Jong, J.C.M., 1997. Verification of the numerical wave model SWAN in the Petten coastal area. Delft, The Netherlands: Delft University of Technology, Master's thesis, 78p.

Dean, R.G. and Dalrymple, R.A., 2004. *Coastal Processes with Engineering Applications*. Cambridge, U.K.: Cambridge University Press, 488p.

Dragani, W.C.; Garavento, E.; Simionato, C.G.; Nuñez, M.N.; Martin, P., and Campos, M.I., 2008. Wave simulation in the Outer Río de la Plata Estuary: Evaluations of SWAN model. *Journal of Waterway, Port, Coastal, and Ocean Engineering*, 134(5), 299–305.

Durrant, T. and Greenslade, D., 2011. *Evaluation and Implementation of AUSWAVE*. Melbourne, Australia: Centre for Australian Weather and Climate Research, Bureau of Meteorology. *Technical Report No. 041*, 55p.

Engelund, F. and Fredsøe, J., 1976. A sediment transport model for straight alluvial channels. *Nordic Hydrology*, 7(1), 296–306.

Etala, P.; Alonso, S.M.; Souto, D.; Romero, R., and Echevarría, P., 2012. Progreso en el modelo de pronóstico de olas hasta un mosaico global multiescala. *XI Congreso Argentino de Meteorología* (Mendoza, Argentina, Universidad Nacional de Cuyo), pp. 125–140.

Fredsøe, J., 1984. Turbulent boundary layers in wave–current motion. *Journal of Hydraulic Engineering*, 110(8), 1103–1120.

Holthuijsen, L.H.; Booij, N., and Herbers, T.H.C., 1989. A prediction model for stationary, short-crested waves in shallow water with ambient currents. *Coastal Engineering*, 13(1), 23–54.

Isla, F.I., 2006. Erosión y defensa costeras. *In:* Isla, F.I and Lasta, C.A. (eds.), *Manual de Manejo costero para la Provincia de Buenos Aires*. Mar del Plata, Argentina: EUDEM, pp. 125–147.

Isla, F.I.; Witkin, G.; Bértola, G.R., and Farenga, M.O., 1994. Variaciones morfológicas decenales (1983–1993) de las playas de Mar del Plata. *Revista de la Asociación Geológica Argentina*, 49(3–4), 55–70.

Jones, O.P.; Petersen, O.S., and Kofoed-Hansen, H., 2007. Modelling of complex coastal environments: Some considerations for best practice. *Coastal Engineering*, 54(10), 717–733.

Kassem, S. and Özkan-Haller, H.T., 2012. Forecasting the wave-current interactions at the mouth of the Columbia River, OR, USA. *In:* Lynett, P. and McKee Smith, J. (eds.), *Proceedings of the 33rd International Conference on Coastal Engineering*. Santander, Spain; Coastal Engineering Research Council. 33, wave paper 53, 7p.

Maia, L.; Jimenez, J.; Serra, J.; Morais, J., and Sanchez-Arcilla, A., 1998. The Fortaleza (NE Brazil) waterfront: Port versus coastal management. *Journal of Coastal Research*, 14(4), 1284–1292.

Mangor, K. and Fuchs, J., 1999. Optimization of port layout with respect to sedimentation, coastal impact, mooring conditions and navigation. *Proceedings of the COPEDEC V* (Cape Town, South Africa), PIANC19p.

Mangor, K.; Brøker, I.; Deigaard, R., and Grunnet, N., 2010. Bypass harbours at littoral transport coasts. *PIANC MMX Congress* (Liverpool, England, PIANC), 18p.

Moorthi, S.; Pan, H.L., and Caplan, P., 2001. *Changes to the 2001 NCEP Operational MRF/AVN Global Analysis/Forecast System*. Washington, DC: National Oceanic and Atmospheric Administration, *Technical Procedures Bulletin No. 484*, pp. 1–14.

Nicholls, R.J.; Larson, M.; Capobianco, M., and Birkemeier, W., 1998. Depth of closure: Improving understanding and prediction. *Proceedings of 26th Conference on Coastal Engineering* (Copenhagen, Denmark, ASCE), pp. 2888–2901.

Padilla-Hernández, R.; Perrie, W.; Toulany, B., and Smith, P.C., 2007. Modeling of two northwest Atlantic storms with third-generation wave models. *Weather and Forecasting,* 22(6), 1229–1242.

Papadopoulos, A.; Katsafados, P., and Kallos, G., 2002. Regional weather forecasting for marine application. *Global Atmosphere and Ocean System*, 8(2–3), 219–237.

Saha, S.; Moorthi, S.; Pan, H.-L.; Wu, X.; Wang, J.; Nadiga, S.; Tripp, P.; Kistler, R.; Woollen, J.; Behringer, D.; Liu, H.; Stokes, D.; Grumbine, R.; Gayno, G.; Wang, J.; Hou, Y.-T.; Chuang, H.-Y.; Juang, H.-M.H.; Sela, J.; Iredell, M.; Treadon, R.; Kleist, D.; Van Delst, P.; Keyser, D.; Derber, J.; Ek, M.; Meng, J.; Wei, H.; Yang, R.; Lord, S.; Van Den Dool, H.; Kumar, A.; Wang, W.; Long, C.; Chelliah, M.; Xue, Y.; Huang, B.; Schemm, J.-K.; Ebisuzaki, W.; Lin, R.; Xie, P.; Chen, M.; Zhou, S.; Higgins, W.; Zou, C.-Z.; Liu, Q.; Chen, Y.; Han, Y.; Cucurull, L.; Reynolds, R.W.; Rutledge, G., and Goldberg, M., 2010. The NCEP Climate Forecast System Reanalysis. *Bulletin of the American Meteorological Society*, 91(8), 1015–1057. doi:10.1175/2010BAMS3001.2.S1

Sclavo, M.; Athanassoulis, G.; Barstow, S., and Cavaleri, L., 2000. An efficient approach to wave climate analysis in coastal waters. *In:* Resio, D.T. (ed.), *6th International Workshop on Wave Hindcasting and Forecasting* (Monterey, California, Environment Canada), pp. 345–360.

Scott, R.D.; Del Core, R., and Murty, T., 2000. Wave climate studies for the Southern Indian Ocean. *In:* Resio, D.T. (ed.), *6th International workshop on wave hindcasting and forecasting* (Monterey, California, Environment Canada), pp. 300–316.

Shields, A., 1936. *Application of Similarity Principles and Turbulence Research to Bed-Load Movement*. Pasadena, California: Soil Conservation Service, 47p., tr. from German by W. P. Ott and J. C. van Uchelen, *Anwendung der Ähnlichkeitsmechanik und der Turbulenzforschung auf die Geschiebe-bewegung*. Berlin, Germany: Mitteilungen der Preussischen Versuchsanstalt für Wasserbau und Schiffbau.

SHN (Servicio de Hidrografía Naval), 1975a. *Carta Náutica H 250, Rada Mar del Plata*. Buenos Aires, Argentina: Departamento de Artes Gráficas, scale 1:50.000, 1 sheet.

SHN, 1975b. *Carta Náutica H 251, Puerto de Mar del Plata*. Buenos Aires, Argentina: Departamento de Artes Gráficas, scale 1:5000, 1 sheet.

SHN, 2004. *Publicación H-216, Avisos a los Navegantes*. Buenos Aires, Argentina: Ministerio de Defensa, Servicio de Hidrografía Naval, *Folleto No. 1*, 84p.

SHN, 2013. *Publicación H-216, Avisos a los Navegantes*. Buenos Aires, Argentina: Ministerio de Defensa, Servicio de Hidrografía Naval, *Folleto No. 8*, 90p.

Sunrise Technical Consultants Engineering Staff, 1971. *Estudio mediante ensayo hidráulico sobre modelo del Puerto de Mar del Plata y sus alrededores*. Tokyo, Japan: Sunrise Technical Consultants, Co., *Technical Report No. 1*, 405p.

Syvitski, J.P.M.; Harvey, N.; Wolanski, E.; Burnett, W.C.; Perillo, G.M.E.; Gornitz, V.; Arthurton, R.K.; Bokuniewicz, H.; Campbell, J.W.; Cooper, L.; Dunton, K.; Gao, S.; Hesp, P.P.; Saito, Y.; Salisbury, J.; Snoussi, M., and Yim, W.W.-S., 2005. Dynamics of the coastal zone. *In:* Crossland, C.J.; Kremer, H.H.; Lindeboom, H.J.; Marshall Crossland, J.I., and Le Tissier, M.D.A. (eds.), *Coastal Fluxes in the Anthropocene: The Land-Ocean Interactions in the Coastal Zone Project of the International Geosphere-Biosphere Programme*. Berlin, Germany: Springer, pp. 39–94.

van Rijn, L.C., 2005. *Principles of Sedimentation and Erosion Engineering in Rivers, Estuaries and Coastal Seas*. Blokzijl, The Netherlands: Aqua Publications, 600p.

□ RESUMEN □

El puerto de Mar del Plata es un importante centro para la industria pesquera en Argentina y se ha convertido en un lugar atractivo para el turismo internacional debido a la reciente construcción de una terminal de cruceros. Sin embargo, el desarrollo de este puerto se encuentra detenido hace varios años debido a persistentes problemas de sedimentación en su canal de acceso y dársenas. Debido a la obstrucción parcial del transporte de sedimentos que provoca la escollera Sur del puerto, el área costera se caracteriza por el avance de la línea de costa aguas arriba, el desarrollo de un banco de arena a través del canal de acceso y significativos procesos de erosión en las playas ubicadas al Norte del puerto. Los mecanismos responsables de estos procesos fueron evaluados mediante el Sistema de Modelación Morfológica MIKE 21/3 de malla flexible desarrollado por la empresa DHI. El modelo morfológico fue calibrado y validado mediante relevamientos batimétricos realizados en el entorno del acceso portuario. El modelo fue aplicado con una simulación a mediano plazo (tres años), con especial interés en la evaluación de la eficacia que tendría una obra de dragado para restablecer la profundidad de diseño del canal. Esta modelación morfológica permitió una mayor comprensión de los principales procesos hidrodinámicos y sedimentológicos que ocurren alrededor de la entrada del puerto, así como la obtención de información potencialmente útil para el diseño de estructuras y la planificación del dragado de mantenimiento. Se determinó que para las presentes condiciones hidrosedimentológicas el banco de arena se mueve hacia el canal de acceso con altas tasas de sedimentación, por lo cual requiere un mantenimiento regular, o la construcción de obras complementarias tales como trampas de sedimentos, espigones, la extensión de la Escollera Sur, etc. Desde el punto de vista de la reducción de la sedimentación, la eficacia de cualquier intervención debe ser verificada antes de su aplicación. En todos los casos, el transporte de sedimentos siempre será bloqueado, con lo cual debe considerarse el bypass artificial de arena con el fin de proteger las playas ubicadas al norte del puerto.